Conformability of wood fiber surface determined by AFM indentation

Dongbo Yan · Kecheng Li

Abstract Mechanical properties of wet fiber surfaces of hardwood chemi-thermo-mechanical pulp and softwood kraft pulp were measured using an AFM as a nanoindetation device. Elastic modulus of wet fiber surfaces was observed in the range of 30 MPa to 1.6 GPa, which is significantly affected by chemical treatment of pulping and bleaching as well as mechanical refining. Plastic yield stress of wet fiber surfaces measured varies from a few MPa to about 100 MPa, and is also highly correlated to chemical and mechanical treatments of these fibers. Plasticity index shows no difference among once-dried hardwood and softwood pulp fibers, but it increases after refining. The dynamic responses of wet fiber surfaces to external loads were evaluated through creep analysis. Even creeps were observed on all wet fiber surfaces, deformation caused by creep is relatively small. The major portion of deformation still comes from instantaneous elastic and plastic deformations. Creep of wet fiber surfaces is a fast dynamic process when subjected to a load change, most of it occurs within several seconds after the initial contact.

Introduction

Wood pulp fibers are renewable materials that have been extensively used for making paper, paperboard, and composites. Fiber–fiber interfaces are of critical importance to

D. Yan · K. Li
Department of Chemical Engineering, University of New Brunswick, Fredericton, NB E3B 5A3, Canada

D. Yan (✉)
Pulp and Paper Division, FPInnovations, 3800 Wesbrook Mall, Vancouver, BC V6S 2L9, Canada
e-mail: Dongbo.Yan@fpinnovations.ca

physical performances of these products because it determines the load-bearing capacity of a fiber network. Fibers are bonded together through intermolecular interactions such as hydrogen bonding and van der Waals forces at fiber–fiber contact surfaces [1]. The inter-fiber bonding strength is determined by the area of molecular contact and the strength of the intermolecular bonds. Inter-fiber bonding arises from the intrinsic tendency of cellulosic fibers to bond to each other when drying. Surface tension forces pull fibers closer together as water is removed from the wet web [2]. Inter-fiber bonds form at the area where surfaces are close enough, or in molecular contact. When two elastic solids with rough surfaces are contacted, the solids will in general not make contact everywhere in the apparent contact area, but only at a distribution of asperity contact spots [3]. Materials with higher roughness, modulus of elasticity and hardness exhibit lower real area of contact. Viscoelastic or viscoplastic deformations and creeps under load would increase the real area of contact as a function of duration of contact. The ability of wet fiber surfaces to deform under capillary pressure becomes critical for forming a real contact area, which is mainly determined by viscoelastic material properties of wet fiber surfaces. However, few studies have been reported so far on quantifying microscopic deformability of wet fiber surfaces [4, 5], even though the importance of it was recognized almost three decades ago [1, 6, 7].

Wood pulp fibers are typical lignocellulosic materials. When subjected to external stresses, two types of responses are normally observed: instantaneous deformation responses against the applied force, and the time-dependent deformation due to the viscoelastic nature of polymers. During a typical papermaking process where water is removed continuously, fibers are subjected to several forces such as capillary force, mechanical compression, and

residual stresses at fiber–fiber interfaces. Therefore, both instantaneous and time-dependent responses should be quantified in order to fully understand the behavior of fiber surfaces.

The objective of this study is to provide a new approach for characterizing microscopic deformability of wet fiber surfaces. Nanoindentation has been widely used for studying elastic modulus of wood cells [8], dry pulp fiber walls [9], fiber–adhesive interfaces [10], and compressibility of wet pulp fibers [5]. In this work, the instantaneous elastic modulus was measured using a classic Oliver–Pharr approach [11]. The dynamic response of fiber surfaces was quantified by creeping behavior and fitting force–displacement curves to a rheological model [12]. However, wood fiber walls are typical heterogeneous, anisotropic biomaterials. Mechanical pulp fibers can be considered as a composite-like material of cellulosic micro fibrils embedded within a lignin matrix, whereas the surfaces of chemical pulp fibers mainly consist of clusters of cellulosic micro fibrils swollen by water. Complex models and experimental methods have been proposed to quantify viscoelastic properties of these materials using indentation techniques [13–15]. For the purpose of comparing differences of fiber surfaces and the effects of mechanical and chemical treatment on them,

"effective" modulus and rheological parameters were used by assuming wet pulp fibers anisotropy and simple continuum surfaces.

Measurement of material properties with nanoindentation

Figure 1 shows typical curves obtained from nanoindentation testing on a typical wet pulp fiber. The top graph of Fig. 1 is a force–time curve during the test showing loading, holding, and unloading phases. The bottom graph of Fig. 1 corresponds to the force–displacement (P–h) curve showing indentation depth and creep deformation during loading, holding, and unloading periods.

Elastic modulus

Since the loading phase of the P–h curve contains both elastic and plastic deformation, the Young's (elastic) modulus, E, of the material can be determined through analyzing the initial part of the unloading curve by assuming that this portion was controlled by purely elastic recovery. This part of the P–h curve can be fitted to the power-law relation as shown in Eq. 1.

Fig. 1 Schematic of indentation depth–time and load–indentation depth curves of nanoindentation of a wet fiber, showing unloading slope, S; maximum indentation depth, h_{max}; final indentation depth at zero load, h_f; and contact depth, h_c
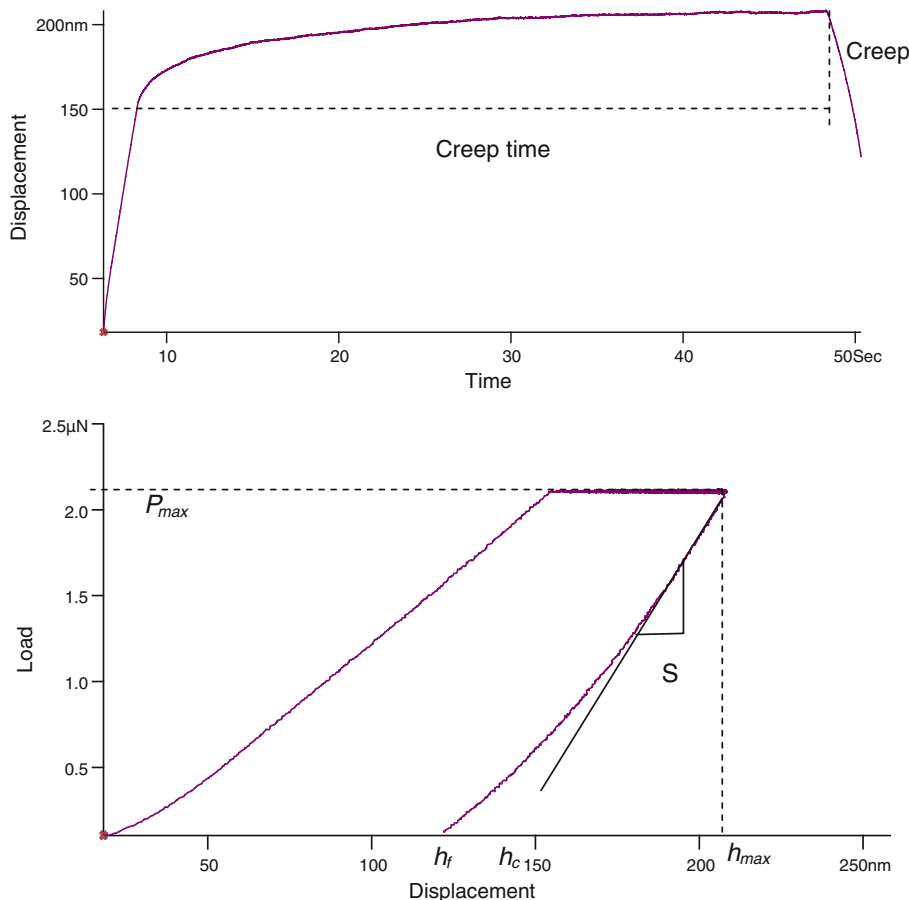
$$P = B(h - h_{\mathrm{f}})^m \tag{1}$$

where P is the applied load, h is the indentation depth, h_{f} is the final displacement, B is a constant, and m is the power-law exponent, which is a function of tip geometry. The pyramid-shaped AFM tip used in this study can be considered as an axis symmetrical indenter [16]. The reduced elastic modulus E_{r} of the AFM tip–fiber surface can be calculated using Eq. 2 according to Doerner and Nix [17].

$$S = \frac{\mathrm{d}P}{\mathrm{d}h} = \frac{2}{\sqrt{\pi}} E_{\mathrm{r}}\sqrt{A} \tag{2}$$

$$\frac{1}{E_{\mathrm{r}}} = \frac{1 - v^2}{E} + \frac{1 - v_0^2}{E_0}, \tag{3}$$

where S is the experimentally measured stiffness of contact as shown in the bottom graph of Fig. 1, E and v are the Young's modulus and Poisson's ratio of the fiber surface, respectively; E_0 and v_0 are the Young's modulus and Poisson's ratio of the indenter tip, respectively; A is the projected area of the elastic contact, which can be calculated from the indenter shape function of the tip. The contact hardness is measured by the peak load P_{max} and the contact area A at the peak load

$$H = \frac{P_{\mathrm{max}}}{A} \tag{4}$$

Oliver and Pharr [11] found that for most materials, the actual contact depth h_{c} is always smaller than the maximum tip displacement h_{max}, and can be estimated using Eq. 5.

$$h_{\mathrm{c}} = h_{\mathrm{max}} - \varepsilon \frac{P_{\mathrm{max}}}{S} \tag{5}$$

$$A = f(h_c) \tag{6}$$

For most indenter tips, the constant $\varepsilon = 0.75$ was recommended as a standard value for indentation analysis [11].

The reduced modulus E_{r} measured with Eq. 2 is based on the assumption that the unloading curve is purely elastic. However, creeping occurs during nanoindentation for most materials, which is a sign of viscoelastic effects [18, 19]. For some soft biomaterials, extreme creeping situations were frequently observed. The viscoelastic creep during unloading can dramatically affect the slope of the unloading curve. The indenter continuously sinks into the specimen even when the load is decreasing, leading to negative values of S in extreme cases [19–21]. In this case, Eq. 2 is no longer applicable. Ngan et al. [18, 20] proposed a correction formula to eliminate creep effect by using a corrected elastic stiffness, S_{e}, instead of experimentally measured stiffness S.

$$\frac{1}{S_{\mathrm{e}}} = \frac{1}{S} - \frac{\dot{h}_{\mathrm{h}}}{\dot{P}_{\mathrm{u}}}, \tag{7}$$

where $\dot{h}_{\mathrm{h}}$ is the tip displacement rate at the end of the load hold just prior to the unloading, and $\dot{P}_{\mathrm{u}}$ is the unloading rate. By using S_{e} instead of S in Eq. 5, E_{r} measured shows good agreement with experimental and finite element simulation results for materials with different power-law viscoelastic situations [20].

Plastic yield stress

The plastic yield stress is measured by identifying the yield point on the loading part of force–displacement curves, assuming the stress σ and strain ε of the material follow the power law

$$\begin{aligned}
\sigma &= E\varepsilon, \quad \varepsilon \le \sigma_y/E \\
\sigma &= K\varepsilon^n, \quad \varepsilon \ge \sigma_y/E,
\end{aligned} \tag{8}$$

where σ_y is the plastic yield stress, K is the work-hardening rate, and n is the work-hardening exponent. For a cone-shaped equivalent indenter on elastic–plastic materials, the indentation force F depends on the indentation depth h, indenter radius R, and the material parameters such as E_{r}, v, n, K [22]. Pure elastic deformation before the plastic yield point can be described using the Hertz contact theory [22]

$$F = \frac{4}{3} E_{\mathrm{r}} R^{1/2} h^{3/2} \tag{9}$$

Once the equivalent stress reaches the yield stress σ_y, plastic yielding occurs and the force–depth curve will start to deviate from the purely elastic indentation curve as illustrated in Fig. 2. Then σ_y is determined by the force and projected area at the yield point.

Plasticity index

A plasticity index ψ is defined as the ratio of irreversible deformation to the overall deformation when a material is subjected to a given external load [23]. It is usually
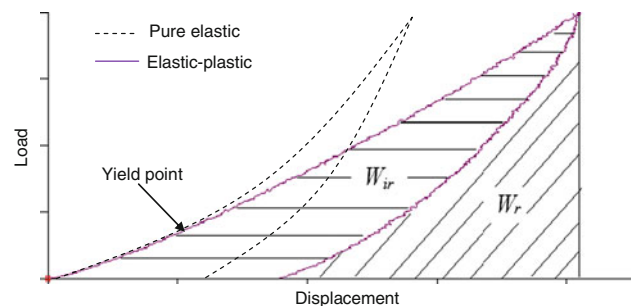
Fig. 2 Schematic plot of load–displacement curve of a typical indentation without holding period. The areas correspond to the reversible (W_{r}) and irreversible (W_{ir}) work. *Dashed curves* represent an ideal elastic material. The plastic yield point is identified by comparing the actual loading curve to that of the ideal elastic one

measured in terms of the ratio of irreversible and reversible work of a load–unload cycle during an indentation test [24]:

$$\psi = \frac{W_{ir}}{W_r + W_{ir}} \qquad (10)$$

where W_{ir} is the irreversible (dissipated) work during the indentation, and W_r is the reversible (stored) work recovered during unloading. They are calculated by the area underneath the loading and unloading portion of the P–h curve as illustrated in Fig. 2. For an ideal indenter tested on a homogeneous material, ψ is expected to be a constant [25]. In this study, ψ is used as a relative index for differentiating the deformation behaviors of papermaking pulp fibers under similar conditions.

Indentation creep test of wet pulp fibers

In addition to instantaneous elastic–plastic deformation, time-dependent creep generally occurs in materials under a constant load over a certain period. Studies found that the creep phenomenon can be well described using standard linear solid models, from which material constants can be extracted by fitting the model to the experimental data [26–29]. However, the solutions to these models are complicated and hard to use from an engineering perspective. Fischer–Cripps proposed a simplified method for nanoindentation creep analysis in a manner suitable for automation calculation without solving the viscoelastic problem at a material level [30]. It is particularly useful for quantifying non-homogeneous materials such as pulp fibers that usually involve hundreds of measurements in order to have a statistically meaningful result. Using Fischer–Cripps' approach, a four-element linear viscoelastic model is used to simulate the response of wet fiber surfaces, which was a combined Maxwell–Voigt five-parameter model as shown in Fig. 3. Assuming a linear viscoelastic material, the response at a constant stress is given by [31]:

$$h(t) = \sigma_0 \left[\frac{1}{E_1^*} + \frac{1}{E_2^*} \left(1 - e^{-tE_2^*/\eta_2} \right) + \frac{1}{\eta_1} t, \right] \qquad (11)$$

where σ_0 is the stress at the beginning of the creep. E_1^* and E_2^* are reduced modulus of the spring element of the Maxwell and Voigt model, respectively; η_1 and η_2 are the viscosities of the dashpot element of two models, respectively. E_1^* is a measure of instantaneous deformation when subjected to an abrupt force, whereas E_2^* controls the degree of retarded elastic deformation caused by creep. η_1 and η_2 are viscosities of the Maxwell model and Voigt model. In the nano indentation using an AFM tip under a constant load, the stress is no longer a constant. The actual stress at creep time t is calculated using the tip area function,
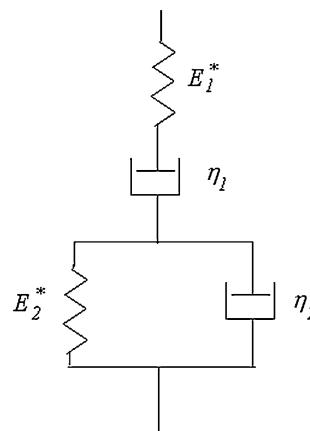

Fig. 3 Four-element combined Maxwell–Voigt model

$$\sigma(t) = \frac{P_0}{f(h_t)}, \qquad (12)$$

where P_0 is the constant load during holding period, $f(h_t)$ is the tip area function and h_t is the indentation depth at creep time t. The temperature-dependent relaxation time is calculated as $\lambda_1 = E_1/\eta_1$, $\lambda_2 = E_2/\eta_2$ for each model. For wet pulp fibers, the creep deformation actually contains both time-dependent viscoelastic and viscoplastic contributions. They are difficult to distinguish during indentation with the method used. Thus a pseudo "pure" viscoelastic creep deformation is used in the model. The time-dependent intrinsic material property is usually characterized by creep compliance $J_c(t)$, which does not depend on the magnitude of the step change of stress in the linear regime and given by [31]

$$J_c(t) = \frac{1}{E_1^*} + \frac{t}{\eta_1} + \frac{1}{E_2^*} \left(1 - e^{-tE_2^*/\eta_2} \right) \qquad (13)$$

Experimental

Materials

Four commercial hardwood pulps and two softwood pulps were used in this study. Hardwood pulps include aspen chemi-themo-mechanical pulp (ACTMP), bleached ACT-MP high tensile grade (AHT) and high bulk grade (AHB), which were obtained from Tembec Inc. (Temiscamingue, QC, Canada). AHT pulps were bleached with a higher alkali charge comparing to that of AHB for the purpose of improving fiber flexibility as well as inter-fiber bonding strength. AHT and AHB pulps were further refined with a PFI mill at 4 % consistency up to 3,000 revolutions, which were denoted as AHTLCR and AHBLCR, respectively. Fully bleached spruce kraft pulp (SBKP) and spruce thermo-mechanical pulp (STMP) were also studied. The

SBKP was refined to 6,000 revaluations with a PFI mill at 10 % consistency and denoted as SBKPPFI.

Sample preparation

Pulp samples (0.3 g o.d.) were diluted to 0.03 % consistency and drained onto a piece of filter paper (Fisher brand Q8) with a TAPPI standard handsheet former. Then pulp fibers were transferred onto a cover slip by placing and gently tapping the filter paper onto a cover slip (Fisher); allowing water to evaporate till free water disappeared. A glass slide (Fisher brand pre-cleaned microscope slide) is coated with a thin layer of solvents free epoxy resin (Devcon, 5 min Epoxy). All excess resin was removed using a blade so that only a very thin resin layer remained on the slide to ensure fibers would only be glued on one side rather than being embedded. The cover slip with fibers is placed on the glass slide. Once the cover slip was removed, some fibers were picked up and fixed on the glass slide by the epoxy resin. When the epoxy cured, the glass slide was immersed in deionized water for use. Since the modulus of epoxy resin is about a few GPa, i.e., 4.6 GPa reported by Adusumalli [9] and 3.1 GPa measured by Gindl and Gupta [32], which is considerably higher than the modulus of most wet fiber surfaces. Therefore, when a very small load was used and the thickness of epoxy layer is much less than fiber wall thickness, the contribution of this epoxy layer to load frame compliance is also small.

AFM indentation

AFM indentations were performed with a standalone AFM (MFP-3D, Asylum Research, Santa Barbara, USA). All measurements were carried out at room temperature (24–26 °C) in aqueous solutions. The ionic strength of solutions is adjusted with NaCl to 0.1 mol/L in order to remove long-range repulsion electrostatic interactions between charged fiber surfaces [33]. All indentations were performed with an Olympus AC160TS silicon probe, which has a nominal spring constant = 42 N/m, elastic modulus $E_0 = 150$ GPa and Poisson's ratio $v_0 = 0.17$. The tip was a three-face pyramidal with nominal tip radius of 9 nm. This tip has a 0° front angle and 35° back angle. The actual spring constant of the cantilever was calculated from the thermal noise with a built-in function of the MFP-3D software [34], which was determined as 45.42 N/m.

Glass slides with fibers were soaked in a NaCl solution for 30 min prior to conducting AFM indentation. Topography mapping of the fiber to be tested was obtained using tapping mode to locate a relatively flat area for force displacement curves measurement. Three groups of indentations were performed at different locations on a fiber surface using three holding times (0, 4, and 40 s). 16 force–displacement curves of the same holding times were
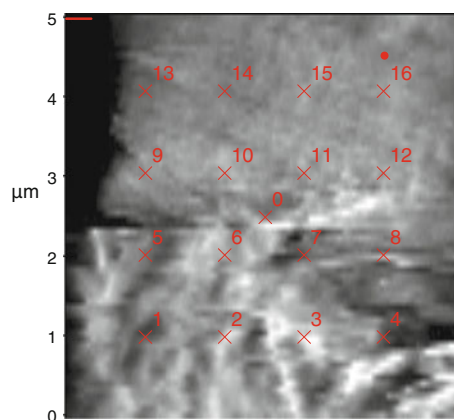
Fig. 4 Locations of force–displacement curves collected on a fiber surface using the force mapping function

measured over a 5 × 5 μm area using force mapping function provided with the AFM control software, which is illustrated in Fig. 4. Then, the tip was moved to a different mapping area to collect force–displacement curves with different holding time.

At least 10 fibers were measured for each pulp sample. The max load $P_{max} = 0.75$ μN was used for all measurements and loading and unloading rates were set to 0.35 μN/s.

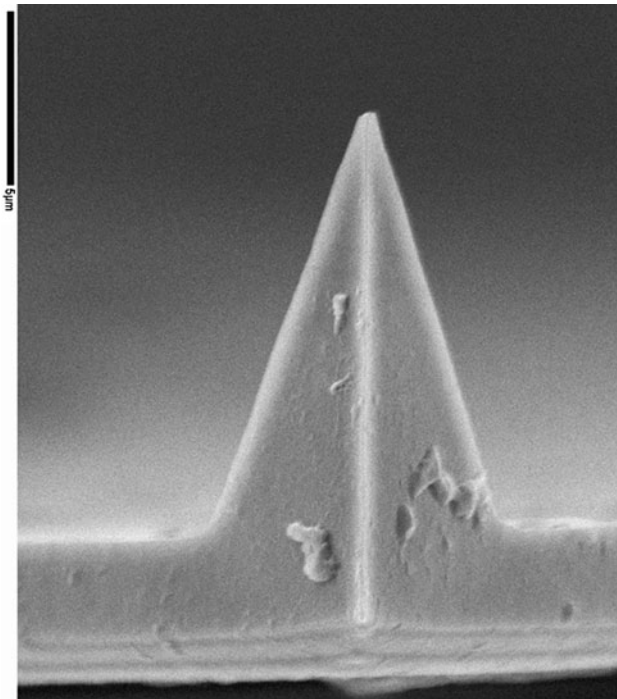### AFM tip shape area function measurement

Since the tip shape area function of the indenter is critical for calculating all material constants, the actual function of the AFM tip was measured with a SEM after all measurements were completed. The width of the three faces of the tip at different height was measured manually on the SEM images as shown in Fig. 5. Then the projected areas at different heights were calculated and fitted with second-order polynomial functions. Once the tip shape area function was determined, it was used as a cone-shaped equivalent indenter in Eq. 8 for detecting plastic yield point.

Data processing

All load–displacement curves were processed with IGOR Pro V6.22 (Wavemetrics inc. Lake Oswego, USA). Plasticity index ψ was measured on P–h curves with zero holding time. Elastic modulus E_r and contact hardness H were measured on curves with 4 s holding time to avoid the effect of delayed elastic deformation using Ngan's approach. The tip displacement rate $\dot{h}_h$ and unloading rate $\dot{P}_u$ in Eq. 7 were calculated on the P–h curve as well.

Plastic yield point is located by fitting the initial part of P–h curves with a power function similar to Eq. 9. The exponent of the function was fixed to 1.5. The yield point on a P–h curve is defined as the point at which the curve

Fig. 5 SEM image of the AFM tip after all measurements have been completed

Fig. 6 Typical load–indentation depth curve obtained on a wet SBKP fiber with $P_{max} = 0.5$ μN and holding time = 4 s
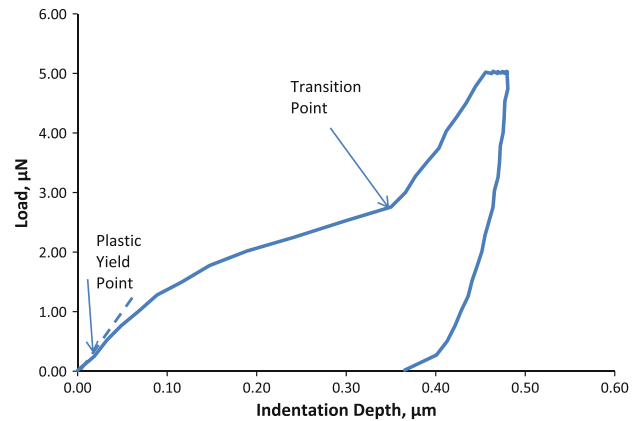
starts to deviate from the purely elastic indentation curve as fitted with Eq. 9. Yield stress is then calculated using force and the projected area of the indenter at the yielding point.

Creep analysis was performed on each P–h curves obtained with 40 s holding time. Using the built-in curve-fitting function of IGOR Pro, all variables ($\eta_1, \eta_2, E_1^*, E_2^*$) in Eq. 11 were estimated. Since the Poisson's ratio of pulp fibers is about $\upsilon = 0.15$ [35], which is close to that of the AFM tips $\upsilon_0 = 0.17$, but the elastic modulus of the tips $E_0 = 150$ GPa is much higher than that of wet fiber surfaces, the reduced elastic modulus E_r is reported directly in this study for comparison purposes.

Results and discussion

Nanoindentation of wet pulp fibers

Figure 6 shows a P–h curve measured on a wet spruce kraft pulp fiber up to a maximum load $P_{max} = 5$ μN. A yielding point was found on the loading curve at $P = 0.25$ μN, indicating the elastic–plastic transition point. A second transition can be observed at $P = 2.6$ μN. The shallow slope before this point indicates a compliant outer region due to fiber swelling. The steeper P–h curve after the transition point indicates the interface between the water-swollen surface layer and the fiber wall substrate. Since this study only focuses on the thin compliant layer on fiber

surface, therefore, a small $P_{max} = 0.75$ μN is used in this study for all measurements to ensure results are obtained only from the outmost layer of wet fibers.

Creeps were observed on all types of wet fibers during holding periods. An AFM height image of a SBKP fiber was scanned immediately after a series of indentations were performed as shown in Fig. 7. Different degrees of pile-up were observed, suggesting that significant plastic deformation occurs during indentation (Fig. 7).

Comparison of elastic modulus of wet pulp fiber surfaces

The average reduced elastic modulus E_r of all pulp fibers measured from the unloading P–h curves using Ngan's approach are listed in Table 1. The mean exponents, m, of all samples were also determined by fitting unloading
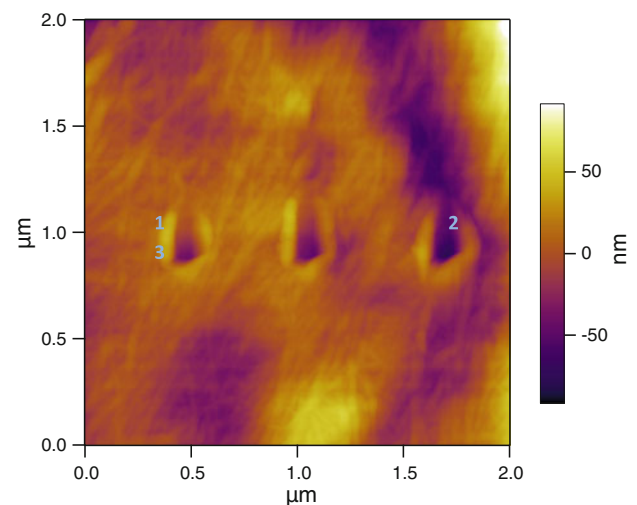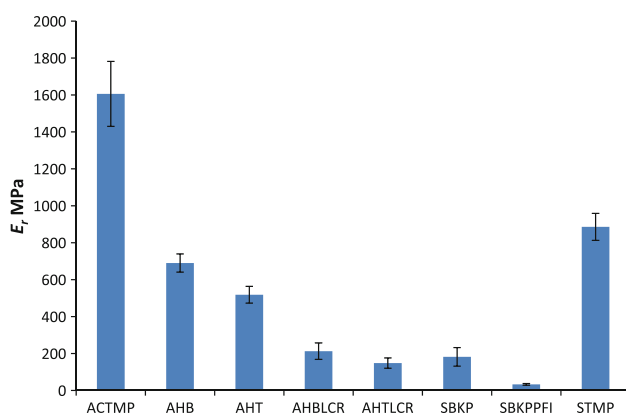

Fig. 7 AFM height image of a SBKP fiber wall after indentation testing. Three pyramidal impressions *1*, *2*, and *3* showing different levels of pile-up under $P_{max} = 0.75$, 1.5, and 3.0 μN, respectively

Table 1 Elastic constants and contact hardness of wet pulp fiber surfaces, with standard error shown in brackets

Pulp sample	M	E_r (MPa)	H (MPa)	Plasticity index (ψ)	σ_y (MPa)
ACTMP	1.72 (0.04)	1606 (176)	1482 (182)	0.64 (0.01)	115 (15)
AHB	1.75 (0.06)	690 (49)	822 (72)	0.63 (0.02)	74 (7)
AHT	1.97 (0.06)	519 (45)	653 (72)	0.64 (0.01)	41 (10)
AHBLCR	2.25 (0.07)	213 (44)	239 (103)	0.72 (0.01)	33 (5)
AHTLCR	2.22 (0.09)	148 (27)	82 (15)	0.71 (0.02)	17 (2)
SBKP	2.27 (0.14)	182 (50)	140 (38)	0.64 (0.03)	7 (1)
SBKPPFI	2.75 (0.12)	33 (5)	18 (3)	0.69 (0.01)	3 (1)
STMP	2.06 (0.09)	886 (73)	1541 (218)	0.64 (0.01)	20 (2)

$P–h$ curves to the power law of Eq. 1. The range of m was found to be from 1.72 to 2.75 for pulp fiber samples measured, which were different to the theoretical values, $m = 2$ for a cone-shaped equivalent indenter [36]. For most pulp fibers, the m determined is within the range of 2.0 ± 0.3, except that of the well-refined SBKPPFI fibers. Large m is an indicator for pile-up during indentation, which usually occurs for "soft" materials with high elastic modulus to yield stress ratio [20]. E_r measured for all samples clearly shows significant differences among different pulp fibers. In general, mechanical fibers have higher E_r than chemical pulp fibers as shown in Fig. 8. For example, STMP fibers have the highest modulus among all spruce pulps, and ACTMP fibers have the highest modulus among all aspen pulps. The STMP fibers were separated at high temperatures without any previous chemical treatment, whereas ACTMP fibers were produced with only mild chemical pre-treatments. Thus, the residual lignin in the cell wall is mostly hydrophobic, which limits the swelling of the fiber wall [37, 38].

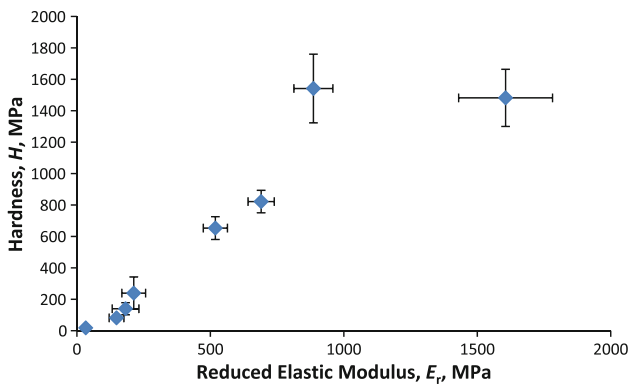Bleaching shows important influence to improving E_r of ACTMP fibers through chemical modification of lignin structures. The fiber surfaces became more hydrophilic after bleaching. E_r of fiber surfaces decreases from 1,606 MPa for ACTMP fibers down to 690 MPa for AHB and 519 MPa for AHT fibers.

Mechanical refining also shows strong impact to E_r of surface layer. The effects of refining on structural properties of fiber walls include the creation of a fibrillated surface structure, breaking the hydrogen bonds between internal fiber layers and fiber swelling and delamination. All those increase conformability of fiber walls as well as fiber wall surfaces, which can be seen from the significant reduction in E_r of AHBLCR, AHTLCR, and SBKPPFI fibers.

The elastic modulus measured with AFM indentation on wet fiber surfaces has been found to be much lower than that of fiber walls. For example, the E_r of ACTMP, AHB, and AHBLCR measured in this study are 1.61, 0.69, and 0.21 GPa, respectively. The elastic modulus of fiber walls measured with wet fiber conformation testing are 17.17, 2.27, and 0.56 GPa, respectively, [39] by measuring the deflection of individual fiber response to external loads. Despite the systematic difference between these two methods, it reveals evidence that a compliance layer exists on fiber surfaces due to swelling and external fibrillation.

Contact hardness H represents overall conformability of wet fiber surfaces under a small load. A nearly linear correlation has been found between H and E_r for fibers used in this study as shown in Fig. 9. Unlike the hardness value measured on dry pulp fibers with nano indentation, which is independent of wood species and bleaching of chemical pulp fibers [9], the hardness measured on wet fiber surfaces is strongly affected by pulping method and bleaching. When a fiber is dry, hydrogen bonding and van der Waals bonding between all elements within fiber walls are strong and form a solid substrate to which stress can be easily transferred. When it is wet, water molecules play a very important role. It decreases intermolecular bonds between cellulose micro fibrils, leads to swollen and soft fiber walls. These functions of water are controlled by chemical compositions and fiber wall structures, which significantly are

Fig. 8 Reduced elastic modulus E_r of wet fiber surfaces measured with nanoindentation, error bars represent standard errors

Fig. 9 Correlation between contact hardness H and reduced indentation modulus E_r of wet pulp fiber surfaces; *error bars* represent standard errors

Fig. 10 Comparison of plastic yield stress σ_y of wet pulp fibers, error bars represent standard errors

Fig. 11 Comparison of plasticity index Ψ of wet pulp fibers

affected by bleaching and refining. An outlier can be found in Fig. 9, which is STMP that has much higher hardness than others. STMP is the only pulp that has not been subjected to any chemical treatment and separated at temperatures nearing the glass transition temperature of lignin. Hydrophobic surfaces caused by unmodified lignin and less structural damage of fiber walls restrict water entering the fiber wall thus restricting swelling. As a result, very high hardness is measured.

Plastic yield stress and plasticity of wet pulp fibers

Plastic yield stress σ_y of materials represents the starting point of local pressure when plastic yield occurs. According to contact mechanics theory, real contact area between rough surfaces is a function of the deformability of said surfaces [3]. For materials with lower σ_y, permanent plastic deformation at asperity–asperity at lower nominal pressure causes much more area in real contact, hence better inter-fiber bonding ability. All σ_y measured are listed in Table 1 and graphically compared in Fig. 10. Similar to elastic modulus, both chemical and mechanical treatments show significant influence on σ_y. SBKP and SBKPPFI fibers have a very low σ_y, less than 7 MPa, which implies that plastic flow easily occurs under capillary pressure at fiber–fiber interfaces during water removal, which results in vary large areas of real contact between fibers.

However, plastic indexes ψ measured show a different pattern than that of σ_y and E_r. A similar plastic index $\psi \approx 0.63$ has been found for most wet pulp fibers, indicating that there is considerable deformation that was not recovered during the unloading cycle of the indentation experiment. Fibers having been mechanically refined such as AHBLCR, AHTLCR, and SBKPPFI, show higher plastic indexes (Fig. 11). It is a result of loosened fiber wall structures and external fibrillations created by refining. Higher ψ implies much more energy has been used to
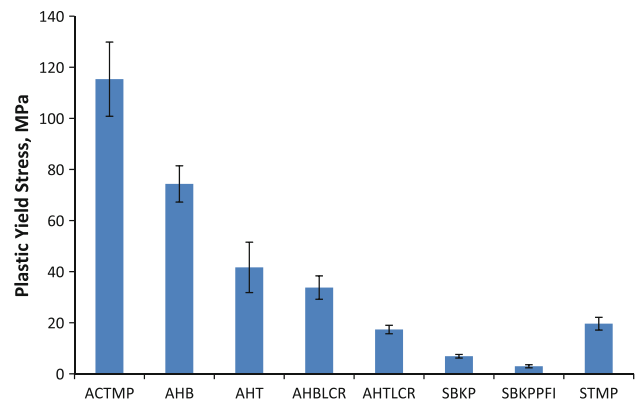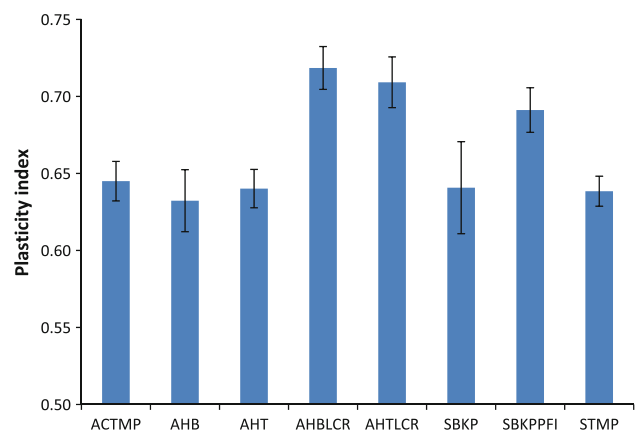
create irreversible deformations at fiber–fiber contacts, and have less residual stress after external loads are released. It should be noted that all pulp fibers used in this study are once-dried. Fiber wall structures are compressed during the drying process. Refining in water will remove this effect, to some degree, and furthermore loosens the fiber wall structure thus increasing its plasticity.

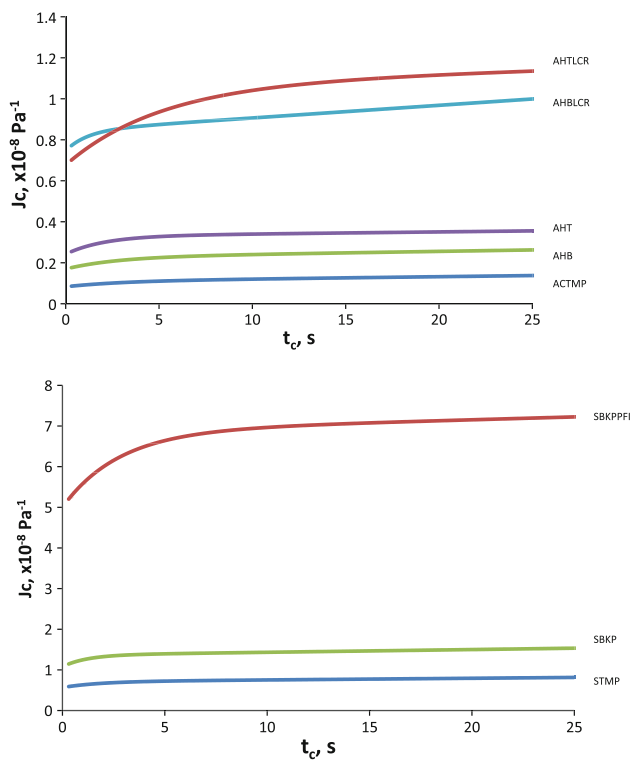Viscoelastic parameters of wet pulp fibers

Individual creep curve obtained was fitted with the Maxwell–Voigt four elements model, which describes dynamic responses of wet fiber surfaces caused by elastic, viscous flow, and retarded elastic deformations. The mean values and standard error of four material constants and time constants of the Maxwell and Voigt models measured for all pulp samples are listed in Table 2.

Simulated creep compliance curves $J_c(t)$ at $P_{max} = 0.75$ μN using material properties in Table 2 are plotted in Fig. 12. The magnitude of $J_c(t = 0)$ simply reflects the relative stiffness of these wet pulp fiber surfaces

Table 2 Viscoelastic constants of wet pulp fiber surfaces, with standard error shown in brackets

Pulp sample	E_1^* (MPa)	E_2^* (MPa)	η_1 (GPa s)	η_2 (GPa s)	λ_1 (s)	λ_2 (s)
ACTMP	1207 (154)	3685 (587)	91 (15)	11.3 (3.1)	75.3	3.1
AHB	590 (122)	1733 (449)	71 (12)	4.8 (0.9)	120.0	2.7
AHT	413 (93)	1130 (316)	100 (33)	2.3 (0.5)	241.5	2.1
AHBLCR	134 (15)	1023 (359)	16 (3)	1.2 (0.2)	120.9	1.2
AHTLCR	148 (6)	257 (12)	35 (7)	1.3 (0.1)	236.7	5.1
SBKP	93 (70)	347 (153)	15 (3)	0.4 (0.06)	160.1	1.2
SBKPPFI	20 (3)	53 (8)	7 (2)	0.15 (0.02)	357.7	2.8
STMP	177 (44)	685 (199)	25 (7)	1.3 (0.3)	138.9	1.8

Fig. 12 Comparison of creep compliance $J_c(t)$ calculated using material constants measured with creep analysis with the AFM tip under step loading to 0.75 μN

deformation, the contribution of creep to overall deformation is relatively small due to higher E_2^*.

The difference in mechanical and chemical treatments of pulp fibers shows significant impacts on instantaneous deformation, but only shows a slight influence to the dynamic characteristics of wet fiber surfaces. Based on this observation, the development of inter-fiber contact area at fiber joints is also a fast process which requires only several seconds.

Conclusions

AFM nanoindentation has been proved to be an effective tool to characterize the surface conformability of wet pulp fibers. Using appropriate methods to compensate pile-ups caused by viscoelastic flow, major material constants such as contact hardness, elastic modulus and plasticity index can be measured on the load–displacement curves. Plastic yield stress of wet fiber surfaces can also be measured by identifying the yield point where P–h curves deviate from the Hertz contact. Measurement results of typical wood fibers clearly reveal changes in the cell wall surfaces caused by pulping, bleaching, and refining conditions, which improve the conformability of wet fiber surfaces significantly.

Indentation modulus, contact hardness and plastic yield stress of wet fiber surfaces are significantly reduced by bleaching and refining. However, changes in plasticity index of wet pulp fibers are mostly affected by mechanical refining.

Creep behavior of wet fiber surfaces can be calculated using a four elements Maxwell–Voigt model. It has been found that the instantaneous deformation is the major type to which wet fiber surfaces respond to external loads. The time constant is small, thus most deformation caused by creep occurs within a short time. However, the creep contribution to overall deformation is relatively small.

when subjected to an abrupt stress change. This instantaneous deformation at beginning of creep is actually controlled by E_1^* of the Maxwell element. E_1^* of all fibers are only slightly smaller than the E_r measured on the initial unloading part of the P–h curve, but much smaller than the E_2^* of the spring of the Voigt element. All these suggest that the instantaneous deformation is a major component of wet fiber surfaces responses to stresses.

For all fibers, the time constant of the Voigt model, λ_2, is much smaller than λ_1 of the Maxwell model. Most of λ_2 are less than 5 s, which suggests that creep of wet fiber surfaces is a fast process. Comparing to the instantaneous

References

1. Elias R, Kaarlo N, Niko N (1998) In: Niskanen K (ed) Paper physics. Fapet Oy, Finland
2. van de Ven TGM (2008) Ind Eng Chem Res 47:7250
3. Persson BNJ (2001) J Chem Phys 115:3840
4. Cheng Q, Wang S, Harper DP (2009) Compos A 40:583
5. Nilsson B, Wagberg L, Gray D (2001) In: Baker CF (ed) Trans 12th Fund Res Symp. Oxford, UK, pp 211–224
6. Ebeling K (1976) 5th Fund Res Symp 1:304
7. Lindström T, Wågberg L, Larsson PT (2005) In: I'Anson SJ (ed) Adv Paper Sci Technol, Trans 13th Fund Res Symp. Cambridge, UK, pp 457–562
8. Gindl W, Schöberl T (2004) Compos A 35:1345
9. Adusumalli R, Mook WM, Passas R et al (2010) J Mater Sci 45:2558. doi:10.1007/s10853-010-4226-9
10. Johannes Konnerth, Wolfgang Gindl (2006) Holzforschung 60:429
11. Oliver WC, Pharr GM (1992) J Mater Res 7:1564
12. Tweedie CA, Van Vliet KJ (2006) J Mater Res 21:1576
13. Bischoff JE (2004) J Biomech Eng 126:498
14. Shen Y-L, Guo YL (2001) Model Simul Mater Sci Eng 9:391
15. Vlassak JJ, Ciavarella M, Barber JR et al (2003) J Mech Phys Solids 51:1701
16. Sirghi L, Ponti J, Broggi F et al (2008) Eur J Biophys 37:935
17. Doerner MF, Nix WD (1986) J Mater Res 4:601
18. Feng G, Ngan AHW (2001) Mater Res Soc Symp Proc 7.1.1
19. Ngan AHW, Tang B (2002) J Mater Res 17:2604
20. Ngan AHW, Wang HT, Tang B et al (2005) J Solids Struct 42:1831
21. Baker SP (2000) Fundamentals of nanoindentation and nanotribology II, vol 649. Materials Research Society, Warrandale
22. Johnson KL (1985) Contactm. Cambridge University Press, London
23. Sakai M (1999) J Mater Res 14:3630
24. Briscoe BJ, Sebastian KS (1996) Proc R Soc A 452:439
25. Iwashita N, Swain MV, Field JS et al (2001) Carbon 39:1525
26. Feng G, Nagn AHW (2002) J Mater Res 17:660
27. Oyen ML, Cook FF (2003) J Mater Res 18:139
28. Vandamme M, Ulm F (2005) Ind J Sol Struct 43:3142
29. Yang S, Zhang Y-, Zeng KY (2004) J Appl Phys 95:3655
30. Fischer-Cripps AC (2004) Mater Sci Eng A 385:74
31. Belfiore LA (2010) In: Belfiore LA (ed) Physical properties of macromolecules. Wiley, New York
32. Gindl W, Gupta HS (2002) Compos A 33:1141
33. Furuta T, Gray DG (1998) J Pulp Pap Sci 24:320
34. Proksch R, Cleveland J (2005) Asylum Research Technical Note
35. Schulgasser K, Page DH (1988) Compos Sci Technol 32:279
36. Oliver WC, Pharr GM (2004) J Mater Res 19:3
37. Li K, Reeve DW (2005) Cell Chem Technol 39:211
38. Li K, Tan X, Yan D (2006) Surf Interface Anal 38:1328
39. Yan D, Li K (2008) J Mater Sci 43:2869. doi:10.1007/s10853-007-2085-9